PHYSICAL REVIEW B **95**, 144423 (2017)

Low-energy magnetoelectric control of domain states in exchange-coupled heterostructures

Muftah Al-Mahdawi,[*] Satya Prakash Pati, Yohei Shiokawa, Shujun Ye, Tomohiro Nozaki, and Masashi Sahashi
Department of Electronic Engineering, Tohoku University, Sendai 980-8579, Japan

(Received 7 December 2016; revised manuscript received 6 February 2017; published 17 April 2017)

The electric manipulation of antiferromagnets has become an area of great interest recently for zero-stray-field spintronic devices, and for their rich spin dynamics. Generally, the application of antiferromagnetic media for information memories and storage requires a heterostructure with a ferromagnetic layer for readout through the exchange-bias field. In magnetoelectric and multiferroic antiferromagnets, the exchange coupling exerts an additional impediment (energy barrier) to magnetization reversal by the applied magnetoelectric energy. We proposed and verified a method to overcome this barrier. We controlled the energy required for switching the magnetic domains in magnetoelectric Cr_2O_3 films by compensating the exchange-coupling energy from the ferromagnetic layer with the Zeeman energy of a small volumetric spontaneous magnetization found for the sputtered Cr_2O_3 films. Based on a simplified phenomenological model of the field-cooling process, the magnetic and electric fields required for switching could be tuned. As an example, the switching of antiferromagnetic domains around a zero-threshold electric field was demonstrated at a magnetic field of 2.6 kOe.

DOI: 10.1103/PhysRevB.95.144423

I. INTRODUCTION

Control of magnetic states by an electrical voltage has garnered a mainstream status in magnetism and spintronics research [1–9] especially for applications in ultra-low-energy technologies of information storage and processing. The most promising techniques rely on voltage control of magnetic anisotropy and coercivity in ferromagnetic (FM) media [1,2,4,6–8]. On the other hand, electric control of magnetic states can also be realized based on magnetoelectric (ME) or multiferroic antiferromagnetic (AFM) media [10,11]. In a heterostructure of ME-AFM/FM exhibiting an exchange bias of the FM, the electrically controlled AFM domain state represents the encoded information. Then, the information is transferred to the FM layer through exchange bias for readout [3,5,12–14], either by a magnetoresistance effect [15], or by the reading head of a storage medium [16,17]. A schematic of the storage concept in comparison to conventional FM-based media is shown in Fig. 1(a) [16,17]. However, the exchange coupling creates an additional energy barrier to magnetization reversal by the applied ME energy. In this paper, we propose and demonstrate a method for low-energy control in exchange-biased ME media.

Chromium oxide (Cr_2O_3) was the first material that demonstrated a linear ME effect [10,18–20]. Cr_2O_3 is a corundum-type collinear AFM with a Néel temperature $T_N = 307$ K, slightly higher than the room temperature. Cr_2O_3 has two possible spin configurations aligned along the c axis of the rhombohedral unit cell, either L^+ $(\uparrow\downarrow\uparrow\downarrow)$ or L^- $(\downarrow\uparrow\downarrow\uparrow)$. The spin configuration is not symmetric under either space inversion or time-reversal operations, and a magnetization M (electric polarization P) is induced by an applied electric E (magnetic H) field. The induced coupling of the electric and magnetic orders is represented by a linear ME susceptibility $\alpha = dM/dE$ $(\alpha = dP/dH)$. ME control of the exchange bias on an FM layer was first demonstrated in single-crystal slabs [3,5]. The recent progress in fabricating high-quality films of Cr_2O_3 by sputtering [21–24] has paved the way for demonstrating ME-controlled film devices [14,25–27]. The control of the AFM domain state is usually extracted from the exchange bias field of a full hysteresis loop of the FM layer [3,5,13,25,28], but this method is impractical for applications. For a full switching of the FM, the coercivity of the FM layer has to be designed to be smaller than the exchange bias field [14,26,27].

The ME properties of Cr_2O_3 films were shown to be close to those of the bulk crystals [29]. However, the required ME energy for switching magnetic domains in films was 3–4 orders of magnitude higher compared to that in bulk single crystals. It can be deduced from the model presented by Borisov *et al.* [3] that the interfacial exchange coupling with the FM layer exerts an additional energy barrier to be overcome by the ME energy [30]. This barrier is inversely proportional to the thickness of the AFM layer [25,28,30]. A dilemma ensues: a small ME switching energy in thin films (20–50 nm) while having a large exchange bias is required for reliable device operation. Recently, a design for ME-based random-access memories without an FM layer was realized, where the induced magnetic polarization in a paramagnetic Pt layer was used for readout [31,32]. We expect that the use of Pt as a detector can be utilized in realizing the proposition outlined by Belashchenko *et al.* of an ME-gated domain wall device [33]. However, the presence of an FM layer is still beneficial for high-density recording. The requirement of an external magnetic field is a limiting factor for establishing ME-based random-access memories, and the ME-based hard-disk media with an FM readout layer is a more suitable candidate [Fig. 1(a)] [16,17].

One of the main features of AFMs is the lack of a net stray magnetization. However, in this work we found a small spontaneous magnetization M_0 that originates within the volume of Cr_2O_3 films from the spin ordering at T_N. This is different from the property of roughness-insensitive boundary magnetization that was theoretically demonstrated for ME AFMs [34]. We utilized the Zeeman energy of M_0 to compensate the energy from an exchange-coupled FM layer, and achieved a switching threshold of Cr_2O_3 domains at a finite magnetic field and a zero electric field.

---

[*] mahdawi@ecei.tohoku.ac.jp

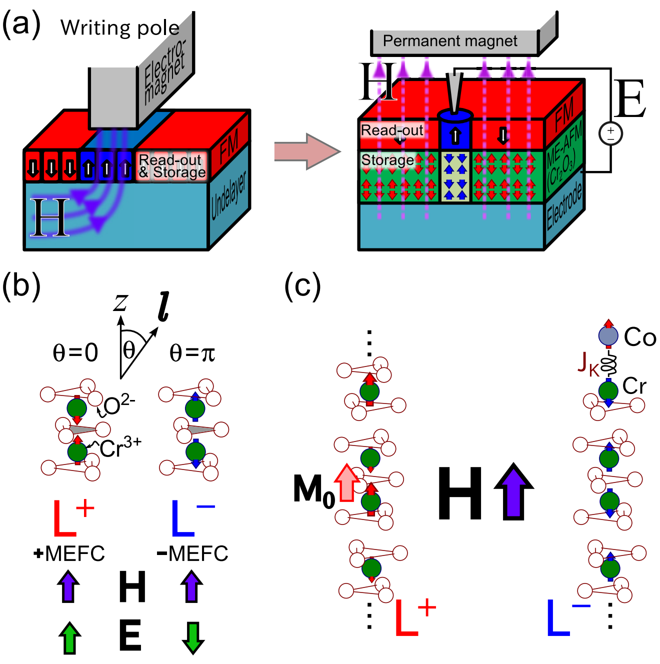

FIG. 1. (a) In contrast to the storage and readout using a single FM layer by a locally varying H in FM-based recording media, in the ME-based media the information retention is in the ME-AFM by a local E and a uniform H, whereas the readout is from an exchange-biased FM. If the FM is designed to have a coercivity smaller than the exchange bias field, a full switching for a practical readout is possible [14,26,27]. (b) Definitions of AFM domains of Cr_2O_3 with respect to the directions of applied fields. The AFM-staggered magnetization vector l is defined as parallel to the spin sublattice beneath the smaller oxygen triangle (grayed triangle area). An angle $\theta = 0(\pi)$ between l and the positive z axis, corresponds to the $L^+(L^-)$ domain. An $L^+(L^-)$ domain results from a parallel (antiparallel) magnetoelectric field cooling, and has a positive (negative) value of magnetoelectric susceptibility α. (c) For a positive magnetic field, the Zeeman energy of Cr_2O_3 spontaneous volume magnetization M_0, which is parallel to l, prefers an L^+ domain (left). On the other hand, the interfacial exchange coupling with the Co ferromagnetic layer favors an L^- domain (right).

II. MODEL OF THE MAGNETOELECTRIC FIELD-COOLING PROCESS

We start by describing a simplified phenomenological model of the switching of AFM domains during magnetoelectric field cooling (MEFC) of Cr_2O_3 films under magnetic field H_{fr} and electric field E_{fr}. We base the model on Ref. [3], by including the effect of M_0 and accounting for thermal fluctuations at T_N. The Cr spins in L^+ (L^-) domain point inward (outward) the shared triangle between the oxygen octahedra [the grayed triangle in Fig. 1(b)] after a +MEFC (−MEFC) [35]. We define the AFM staggered magnetization vector l as parallel to the sublattice spin beneath the shared oxygen triangle. Hence, the angle between l and $+z$ direction θ is $0\,(\pi)$ for L^+ (L^-) domain state [Fig. 1(b)]. The dominance of either $L^\pm$ domain is determined by the energies affecting the AFM layer at T_N [3]. The relevant energies are the ME energy W_{ME}, the Zeeman energy of Cr_2O_3 magnetization W_{ZM}, and the exchange coupling to the FM layer W_{EX}. We consider the film to be an ensemble of uncorrelated particles at T_N, and each of them contains a single uniform classical spin within a short-range-order volume V set by the grain size [36]. Then the total free energy in cgs units for a single particle is

$$\begin{aligned} W/V &= W_{\mathrm{ME}} + W_{\mathrm{ZM}} + W_{\mathrm{EX}} \\ &= -\alpha E_{\mathrm{fr}} H_{\mathrm{fr}} \cos\theta - M_0 H_{\mathrm{fr}} \cos\theta + \frac{J_K}{t}\cos\theta \\ &\equiv W_0 \cos\theta, \end{aligned} \tag{1}$$

where M_0, t, and J_K are the magnetization per unit volume, the thickness of the AFM layer, and the exchange-coupling energy between the FM and AFM layers at the interface. For simplicity, θ is assumed to be uniform along the z direction. This simplification is more valid for high H_{fr}, as W_{ZM} and W_{ME} will be much larger than W_{EX}. The macroscopic values of M_0, J_K, and α at T_N are zero. However, this is due to the thermal averaging of the order parameter [37,38]. Equation (1) describes the energy of single-domain particles smaller than the short-range-order length at T_N. Therefore, the effective values of M_0 and J_K in Eq. (1) should be close to the measurable values at a low-temperature limit. On the other hand, due to the larger thermal fluctuations at T_N, the exchange-driven $\alpha(T_N)$ on a single-particle scale should be larger than the macroscopic peak value at 240–270 K. The choice of signs in Eq. (1) is such that the sign of W_{ME} produces an L^+ (L^-) domain for a positive (negative) product of E_{fr} and H_{fr}. The signs of W_{ZM} and W_{EX} were chosen to prefer l parallel and antiparallel to H_{fr}, respectively [Fig. 1(c)]. J_K is defined as positive for an antiparallel coupling between FM's magnetization and l. The reasoning for these choices is based on the experiments and discussions presented latter.

During the transition from the fluctuating state to the ordered state at T_N during cooling, the AFM domains are stabilized within a few kelvins below T_N by an increase of the crystalline anisotropy barrier [36]. The condition for the preferable domain is $\partial^2 W/\partial\theta^2 > 0$. An L^+ (L^-) domain is more stable when $W_0 < 0$ ($W_0 > 0$). At the switching threshold condition of $W_0 = 0$, an equal number of $L^\pm$ domains are present. For a fixed H_{fr}, the threshold electric field for switching E_{th} is

$$\begin{aligned} E_{\mathrm{th}} &= -\frac{M_0}{\alpha} + \frac{J_K}{\alpha t}\frac{1}{H_{\mathrm{fr}}} \\ &\equiv E_M + \frac{E H_J}{|H_{\mathrm{fr}}|}. \end{aligned} \tag{2}$$

The absolute value of H_{fr} in Eq. (2) is to account for the switching of the FM spin direction by a negative H_{fr}, and hence a change in the sign of W_{EX}.

The E_{th}-$1/H_{\mathrm{fr}}$ plot is a line with a slope determined by the strength of J_K/t [3,26]. For thinner Cr_2O_3 films and a stronger exchange bias of the FM layer, a higher electric field is required compared to thick slabs with a weak exchange bias [3,14,25–27]. However, with the presence of $M_0 \parallel l$, a negative y intercept is found. Therefore, a zero E_{th} can be realized at a finite magnetic field H_{E0}. At H_{E0}, the Zeeman energy of M_0 balances the exchange-coupling energy J_K/t. Then a small electric field can be used to choose either of the AFM domain states, and the dilemma between having a higher J_K/t ratio and lower electric and magnetic fields is resolved.

The probability of switching after MEFC is found from the averaged domain state $\langle L \rangle$

$$\langle L \rangle \equiv \frac{v^+ - v^-}{v^+ + v^-}, \tag{3}$$

where $v^{\pm}$ are the volume proportions of $L^{\pm}$ domains. The probability distribution P_Θ of θ for each particle at T_N is given by

$$P_\Theta(\theta) = \frac{W_0 V}{\sinh(W_0 V)} \sin\theta \exp\left(\frac{-W_0 V \cos\theta}{k_B T_N}\right), \tag{4}$$

where k_B is the Boltzmann constant, and $W_0 V/\sinh(W_0 V)$ is the normalization factor. As the AFM domains are forced into either domain state by the anisotropy barrier, the switching probability $\langle L \rangle$ after MEFC can be found as the expectation value of $g(\theta) = \mathrm{sgn}(\theta - \pi/2)$, where sgn is the signum function, as follows:

$$\begin{aligned}\langle L \rangle &= \int_0^\pi g P_\Theta d\theta = \tanh\left(\frac{-W_0 V}{2k_B T_N}\right)\\ &\equiv \tanh\left(\frac{E_{\mathrm{fr}} - E_{\mathrm{th}}}{\lambda_E}\right),\end{aligned} \tag{5}$$

where the finite probability of switching around E_{th} is described by λ_E:

$$\lambda_E = \frac{2k_B T_N}{\alpha V}\frac{1}{H_{\mathrm{fr}}} \equiv \frac{EH_T}{H_{\mathrm{fr}}}. \tag{6}$$

III. EXPERIMENTAL VERIFICATION

We compared the presented model with experimental observations made on deposited films and a bulk slab of Cr_2O_3. The description of samples preparation, structural characterizations, and measurement setup were reported elsewhere [23,29,36]. Sputter-deposited films of Pt (25)/Cr_2O_3 (500)/top layer were prepared over *c*-Al_2O_3 substrates, where the numbers in parentheses are the calibrated thicknesses in nanometers. Two types of films were prepared. In the film sample woEB (without exchange bias), a single Pt (25) top layer was deposited. In the film sample wEB (with exchange bias), the top layer was an FM exchange coupled through a metal spacer, with the composition of Pt (1.1)/Co (1)/Pt (25). The magnetic and magnetoelectric properties were measured by a magnetometer based on a superconducting quantum interference device. The average domain state was determined from measurements of peak α in the setup described in Ref. [36]. The parallel ME susceptibility α was measured by applying an out-of-plane ac electric field and measuring the in-phase component of the electrically induced magnetization of the Cr_2O_3 films [29,39]. In contrast to measuring the exchange bias on the FM layer, the present scheme has the benefit of probing the AFM domain state inside the film, regardless of the presence of an FM layer (Appendix A). The low-temperature limit of exchange-bias in the sample wEB was 570 Oe, corresponding to $J_K = 8\times10^{-3}$erg/cm^2 (Appendix B).

The temperature dependence of the thermoremnant magnetization (TRM) at zero field after a magnetic-field cooling was measured for various thicknesses of Cr_2O_3 with Pt capping, and the samples area was measured by a calibrated optical microscope. The magnetization areal density showed a linear dependence on thickness, with a slope of 0.3 emu/cc [Fig. 2(a)]. After the removal of capping by Ar^+ ion milling, no significant change of magnetization was found [blue squares in Fig. 2(a)]. This indicates that the origin of M_0 is dominated by a volume component, and not from a surface magnetization. The fully polarized surface should have an estimated areal magnetization of 8×10^{-6} emu/cm^2 that is thickness independent [dashed green line in Fig. 2(a)] [40]. TRM switched in the same direction as H_{fr} [Fig. 2(b)]. The temperature dependence of α also switched with the direction of H_{fr} [Fig. 2(c)]. At 240 K, α was positive (negative) for a positive (negative) H_{fr}. Therefore, the bulk M_0 is parallel to l [the left-hand side of Fig. 1(c)]. The AFM domains are coupled to H_{fr} through M_0 (Appendix C), and the Zeeman energy prefers $l \parallel H_{\mathrm{fr}}$. Furthermore, both the spontaneous magnetization and the AFM order became zero at the same transition temperature of 298 K. The inset of Fig. 2(c) shows TRM and α measured for the same cut of the sample woEB.

No other phases of chromium oxide were found by x-ray diffraction analysis [22,23,29], and the oxidation state of Cr ions was close to +3 as confirmed by x-ray photoelectron spectroscopy and x-ray absorption near the edge structure (data not shown). All these mean that the observed spontaneous volume magnetization originates from the ordering of Cr spins in Cr_2O_3. As a speculation on the origin, we should consider the magnetic moments on each sublattice. The magnetic moments of Cr ions are reduced from an expected maximum of 3 μ_B, due to the charge back transferred from oxygen 2*p* orbitals into Cr 3*d* orbitals [41]. In the sputtered films, the unit cell is distorted and strained [22,29]. It is likely that the atom coordinates of fabricated films are changed from bulk values. The different bond lengths and angles of Cr-O can give a different magnetic moment per sublattice. This would result in a ferrimagnetic-type order, represented by different arrow sizes in Fig. 1(c). The corresponding change in Cr magnetic moments needs to be $2\times10^{-3}\mu_B$ per ion to account for M_0. The relative orientation of M_0 as parallel or antiparallel to l depends on the details of which sublattice is dominant. Alternatively, Kosub *et al.* [32] attributed a similar observation of a ferrimagnetic order in Cr_2O_3 films to uncompensated spins at misfit dislocations during the initial growth. To explain our results accordingly, defects that prefer the spins from one sublattice should be postulated inside the film.

The relation between the direction of Co magnetization and the Cr_2O_3 AFM vector is antiparallel based on two considerations. First, it was reported that the Cr and Co spins are antiferromagnetically exchange coupled [42]. The second consideration is that corundum-type crystals prefer to terminate in the bottom half of the buckled metal-ion layer for most fabrication conditions [43,44]. This termination corresponds to the lower spin sublattice of Fig. 1(b). Therefore, the direction of Cr_2O_3 surface spin is parallel to l. The combination of the previous two observations indicates a preference of an L^- domain by the exchange coupling to Co spins for $H_{\mathrm{fr}} > 0$ [the right-hand-side of Fig. 1(c)]. Figure 2(d) shows the measurement of the direction of AFM domains in relation to H_{fr} for the sample wEB. The negative (positive) α_{peak} for a positive (negative) H_{fr} indicates that L^- (L^+) domains are stabilized by coupling to Co spins [Fig. 2(d)]. Hence, the exchange coupling prefers an antiparallel relation

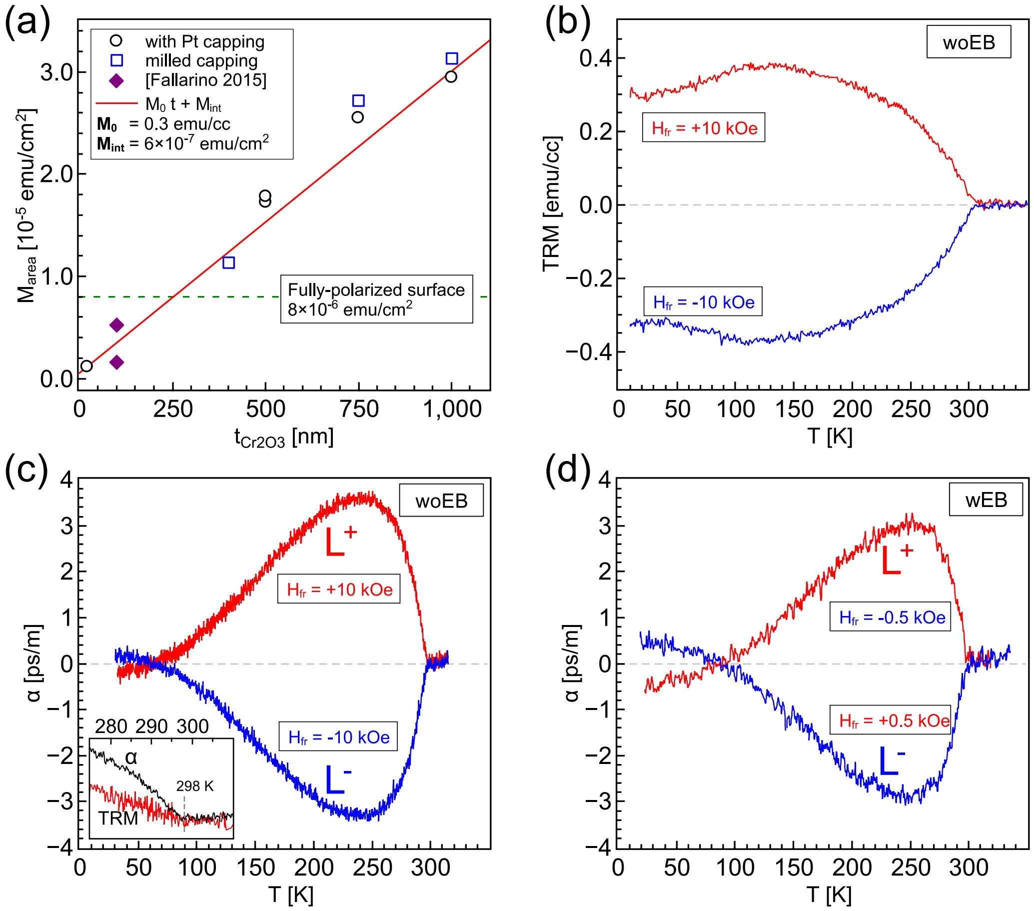

FIG. 2. (a) The magnetization areal density of Cr_2O_3 films shows a linear dependence on thickness, with a negligible surface component. The dashed line is the maximum expectation from a thickness-independent fully polarized surface magnetization. The magnetization values from Ref. [40] are also plotted, but not included in the fitting. (b), (c) The temperature dependence of (b) the thermoremnant magnetization (TRM), and (c) the magnetoelectric susceptibility α of the sample without an exchange bias (woEB) after cooling in a positive and a negative H_{fr}. The inset in (c) shows coinciding transition temperatures from TRM and α. (d) The temperature dependence of α, for the sample wEB. (c), (d) For the same direction of H_{fr}, the opposite Cr_2O_3 domains are generated in the samples woEB and wEB.

between l and H_{fr}. More confirmation on the coupling sign between Co and Cr_2O_3 domains is presented in Appendix A. The sign of coupling did not change by changing the material of metal spacer or by removing the spacer.

Between the two AFM domain states $L^{\pm}$, the sign of α changes but with the same magnitude. Therefore, the normalized α by the saturation value gives the average domain state as $\langle L\rangle = \alpha_{\mathrm{peak}}/\alpha_{\mathrm{max}}$. Figure 3(a) shows the temperature dependence of α for the sample woEB after MEFC under $H_{\mathrm{fr}} = 10$kOe and a variable E_{fr}. For the whole range of temperatures, α changes linearly between two opposite maxima, and the dependence of normalized α on cooling fields is temperature independent. Thus, it is suitable to estimate $\langle L\rangle$ from measuring only the normalized peak value at 240 K. The measurement was performed after MEFC at H_{fr} and E_{fr} fields from 320 K, which is higher than T_N, down to the detection temperature of 240 K. α is presented in ps/m for consistency with other reports. The peak-to-peak noise level was $<5\times10^{-9}$ emu, and the measurement was averaged over a 3-min span.

The measurements of $\langle L\rangle$-E_{fr} curves were used to find E_{th} from fittings to Eq. (5) for a varying H_{fr} [Fig. 3(b)]. The data points were taken at a random sequence, and no effect of points ordering was found. The left-hand side of Fig. 3(b) shows $\langle L\rangle$-E_{fr} dependence of the sample woEB. A gradual switching between the positive and negative maxima was found, with a tendency closely resembled by Eq. (5). E_{th} is at a constant -137 kV/cm, not dependent on H_{fr}. During cooling in a positive H_{fr}, an additional negative electric field is needed so that the negative magnetoelectric energy favoring the L^- state overcomes the Zeeman energy of M_0 favoring the L^+ state. As the magnetic field is increased, both Zeeman and magnetoelectric energies increase by the same amount. Therefore, E_{th} is not dependent on H_{fr} [the red squares in Fig. 3(c)]. In comparison, a bare 0.5-mm slab of a single-crystal Cr_2O_3 had a zero E_{th} irrespective of $1/H_{\mathrm{fr}}$, due to the absence of M_0 and J_K [the blue diamonds in Fig. 3(c)]. In the sample wEB, the $\langle L\rangle$-E_{fr} dependence shifts with H_{fr} due to the presence of J_K [Fig. 3(b)]. At $H_{\mathrm{fr}} \approx 2.6$ kOe, the $\langle L\rangle$-E_{fr} curve is symmetric around a zero E_{fr}. This demonstrates that low-voltage switching at a finite magnetic field is possible. The shift of E_{th} is linear with $1/H_{\mathrm{fr}}$ [the black circles in Fig. 3(c)], and the y intercept is in agreement with the sample woEB. From Eq. (2), the x intercept corresponds to $H_{E0} = J_K/(M_0 t)$.

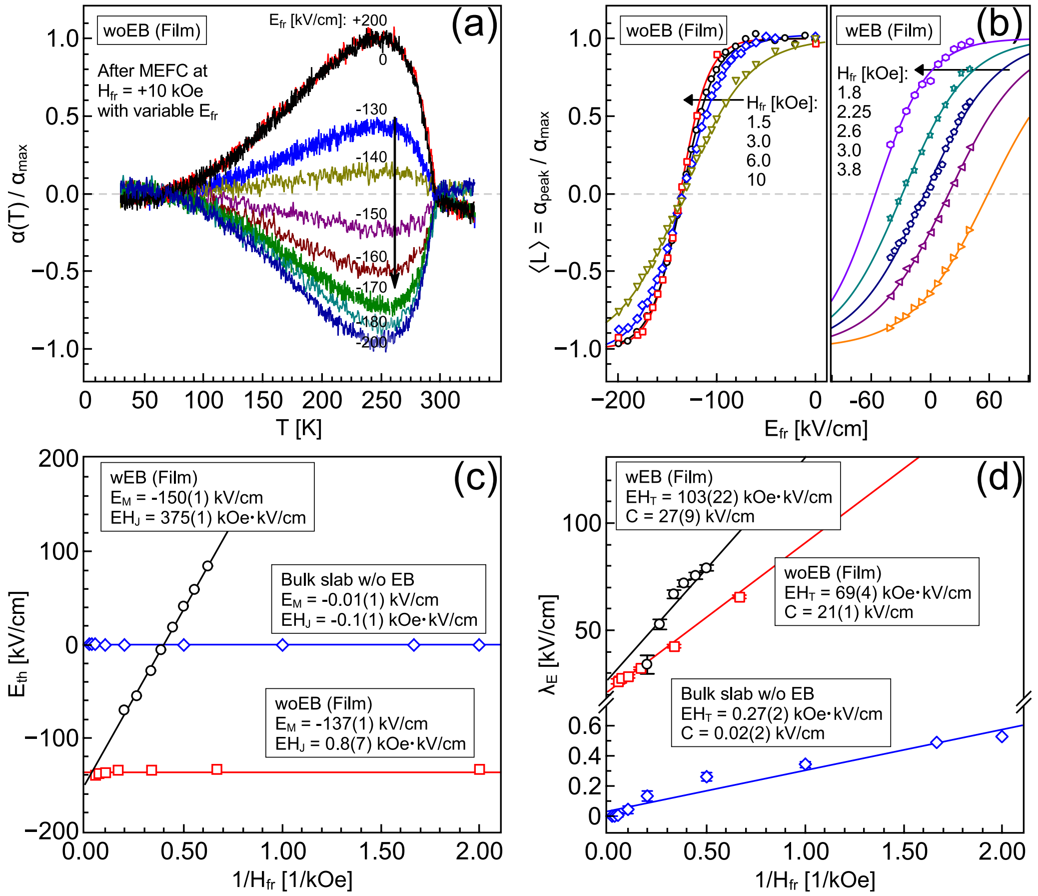

FIG. 3. (a) The temperature dependence of α in the sample woEB, normalized by the maximum peak value for a cooling under the simultaneous application of a magnetic field $H_{\mathrm{fr}} = +10$ kOe and a varying electric field E_{fr}. An additional negative E_{fr} was needed to switch the $\mathrm{Cr_2O_3}$ domains. (b) A comparison of the dependence of the average domain state $\langle L \rangle$ on E_{fr} between the samples woEB and wEB. The sample woEB shows a constant threshold electric field E_{th}, irrespective of H_{fr}. The sample wEB has a shift of E_{th} with changing H_{fr}. At $H_{\mathrm{fr}} \approx 2.6$ kOe, the switching curve has a zero E_{th}. (c) Plots of E_{th}-$1/H_{\mathrm{fr}}$ with fits to the model outlined in Eq. (2). A single-crystal slab of $\mathrm{Cr_2O_3}$ has a zero E_{th} regardless of $1/H_{\mathrm{fr}}$ (blue diamonds). The samples wEB and woEB have similar negative y-intercepts, due to the presence of M_0 (black circles and red squares, respectively). For the sample wEB, a slope results from exchange coupling to Co, and a zero E_{th} is found at H_{E0}. (d) The dependence of λ_E on $1/H_{\mathrm{fr}}$ is linear with a slope EH_T that is determined by αV. For the deposited films, a nonzero λ_E is still present even in the vanishing $1/H_{\mathrm{fr}}$ limit (C).

An estimation from the low-temperature values of J_K and M_0 gives $H_{E0} \approx 5.3$ kOe. Considering the approximations in the macrospin model, the experimental value of $H_{E0} = 2.6$ kOe has a reasonable agreement. The presence of M_0 can be used to estimate the effective α at T_N during MEFC from $E_M = -M_0/\alpha$, which is estimated at 27 ps/m.

Next, we turn to the smooth switching around E_{th}, represented by λ_E. λ_E characterizes the required $|E_{\mathrm{fr}} - E_{\mathrm{th}}|$ for a saturation of the switching probability. It is linearly proportional to $1/H_{\mathrm{fr}}$, where the proportionality constant is the thermal fluctuation energy translated into ME energy $EH_T = 2k_B T_N/\alpha V$. Figure 3(d) shows the λ_E-$1/H_{\mathrm{fr}}$ plot for both of the samples wEB and woEB (black circles and red squares, respectively). The slope of λ_E-$1/H_{\mathrm{fr}}$ line is finite, corroborating the finite value of αV. However, a nonzero λ_E is found when $1/H_{\mathrm{fr}}$ approaches zero. For a higher H_{fr}, the switching probability should saturate for a smaller $|E_{\mathrm{fr}} - E_{\mathrm{th}}|$ due to the larger ME energy. However, short-ranged paramagnetic spin waves are reported to be excited at the phase-transition temperature or at a higher temperature [45,46]. Spin-wave fluctuations with energy that is dependent on $H_{\mathrm{fr}} M_0$ can explain why a nonzero $|E_{\mathrm{fr}} - E_{\mathrm{th}}|$ is still needed at a high H_{fr} in the sputtered films. Due to the large V of the single-crystal slab and the absence of M_0, a line with a much smaller slope and no intercept was found [blue diamonds in Fig. 3(d)].

IV. CONCLUSIONS

In this work, we described the magnetoelectric switching of the antiferromagnetic domains of $\mathrm{Cr_2O_3}$ films by using a phenomenological model, and compared it with direct measurements on the average domain state after cooling in magnetic and electric fields. The model is based on the observation of a competition between the Zeeman energy of a spontaneous volume magnetization of $\mathrm{Cr_2O_3}$ sputtered films, and the exchange-coupling energy with a proximate ferromagnetic layer. We found that the volume magnetization of $\mathrm{Cr_2O_3}$ films caused an opposite shift in the required electric field for switching compared to the shift caused by the exchange coupling. At the point of balance, low values of the writing electric field were achieved that are symmetric around a zero threshold value. We expect that such a development can pave the way for controlling both the writing energy and the exchange bias in heterostructure-based magnetoelectric and multiferroic information media.

ACKNOWLEDGMENT

This work was partly funded by the ImPACT Program of the Council for Science, Technology and Innovation (Cabinet Office, Government of Japan).

APPENDIX A: COUPLING SIGN OF CO AND Cr_2O_3 DOMAINS AND THE LINEARITY OF MAGNETOELECTRIC SUSCEPTIBILITY α

We measured the ME effect in the sample wEB after magnetic-field cooling. The simultaneous measurement of the dc and ac responses of the SQUID magnetometer along the detection coils is shown in Fig. 4(a). The measurement was at 240 K with +500 Oe applied along the detection coils after magnetic-field cooling (MFC) under +500 Oe from 320 K. The shape of the response was typical for a second-order gradiometer. The M_{dc} is mainly coming from Co due to its high saturation magnetization. The direction of Co magnetization

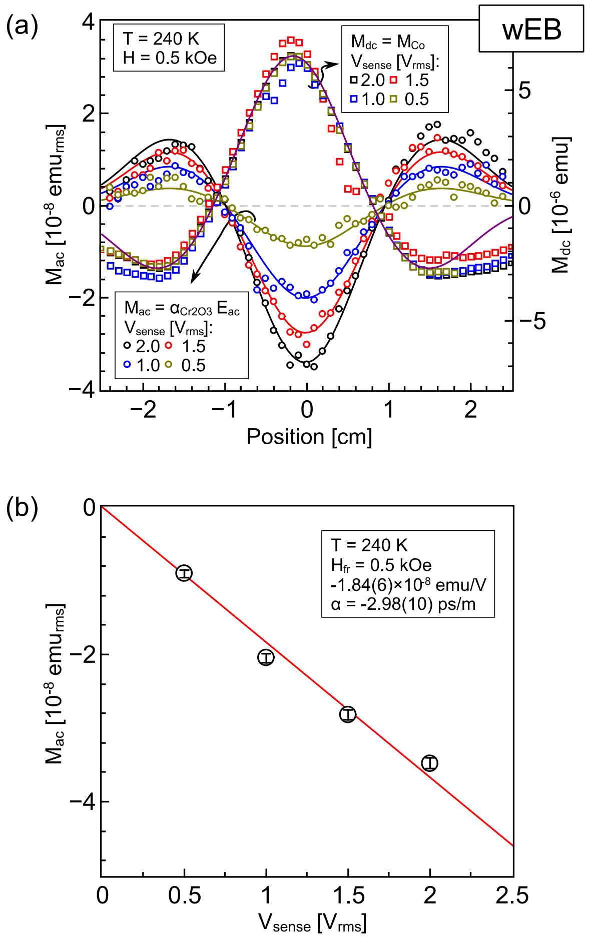

FIG. 4. (a) The dc (squares) and ac (circles) responses of the SQUID magnetometer along the position of the sample relative to the detection coils. The sample wEB was used, and the measurement was after MFC at +500 Oe. The dc and ac magnetizations correspond to Co's magnetization and Cr_2O_3 ME response, respectively. (b) The magnitude of M_{ac} increased linearly with sensing voltage, indicating that the ME response is linear. The negative sign of α indicates the formation of L^- domains.

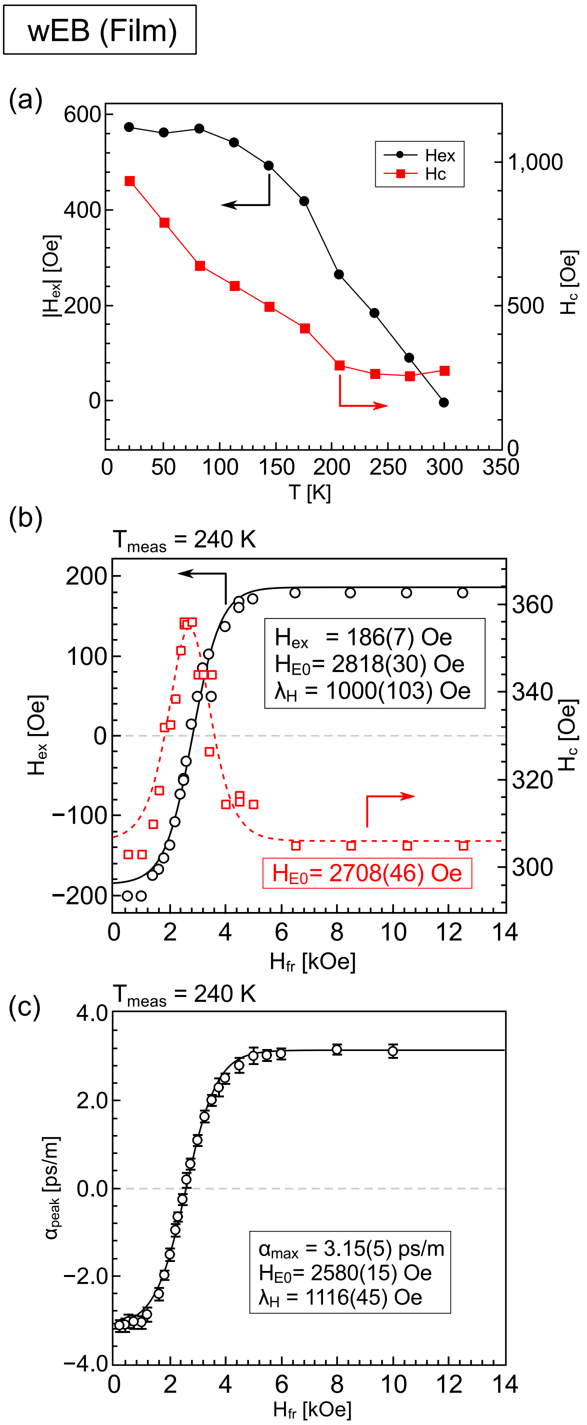

FIG. 5. (a) The temperature dependence of exchange-bias field H_{ex} and coercivity H_c of Co. (b) The change of H_{ex} and H_c against H_{fr}. The solid black line is a fitting to Eq. (B1), whereas the dashed red line is an eye guide. (c) The dependence of α of Cr_2O_3 on H_{fr}, with a fitting to Eq. (B1). (b), (c) The fitting results from H_{ex} and α measurements are consistent, indicating that the AFM domains at the surface and inside the Cr_2O_3 film are highly correlated.

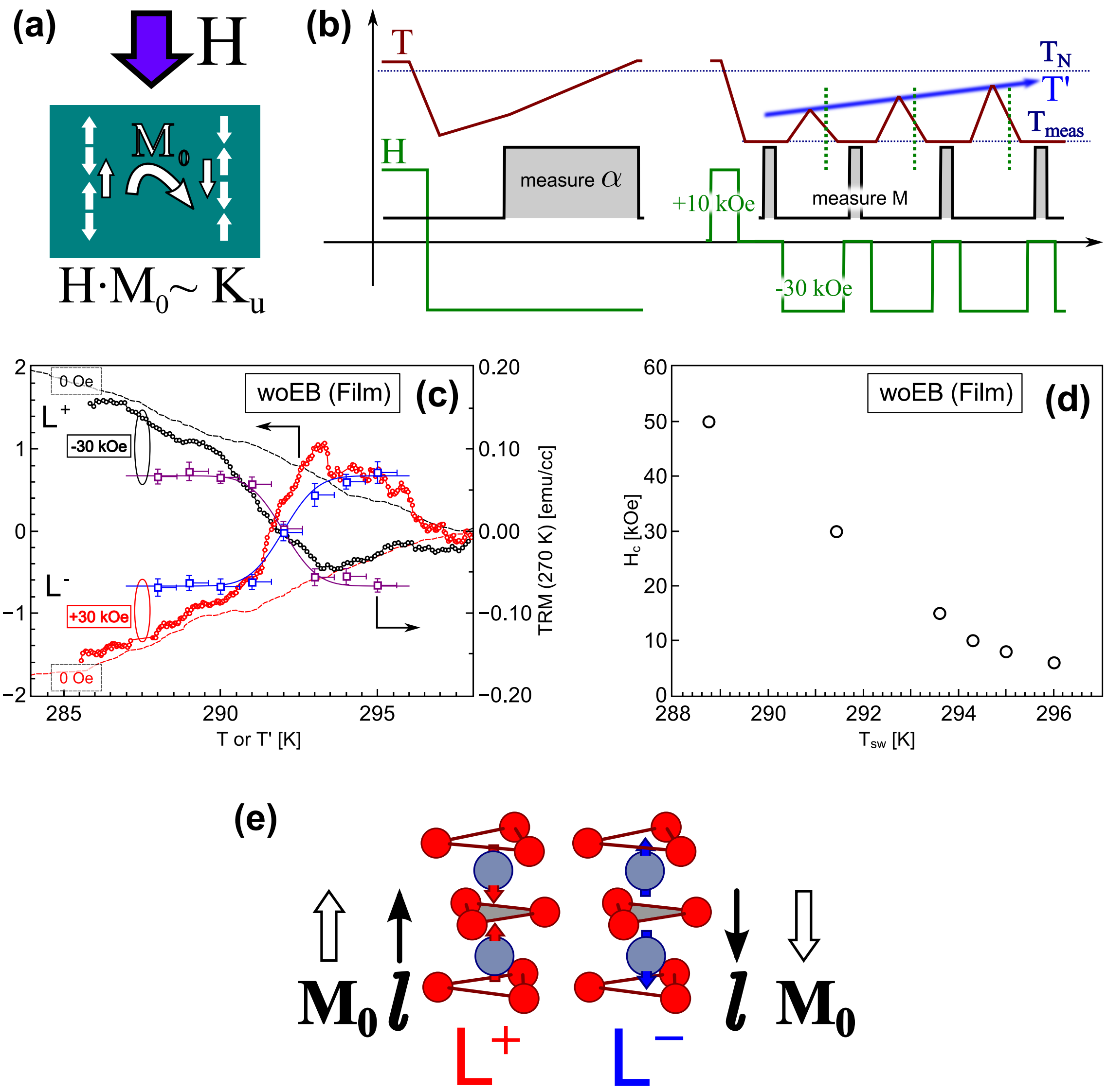

FIG. 6. The relation between the AFM order parameter l and Cr_2O_3 magnetization M_0 is parallel. (a) After initializing in one domain state, applying an opposing H will switch the AFM domains through coupling to M_0, when anisotropy K_u is low. (b) The protocols for measuring the switching of l and M_0 are shown. (c) Applying ∓ 30 kOe to a $L^{\pm}$ domain induces a sign reversal in α and M_0 at the same temperature T_{sw}. Horizontal error bars correspond to temperature overshoots when T' is reached. (d) The temperature of switching at an applied field corresponds to the coercivity H_c at that temperature. The large change of H_c vs T_{sw} is due to a small M and a large decrease in K_u around T_N. (e) A schematic showing that l is parallel to M_0.

is parallel to H_{fr} as expected. The $M_{\mathrm{ac}} = \alpha_{\mathrm{Cr2O3}} E_{\mathrm{ac}}$ is from the ME effect of Cr_2O_3 layer. The sign of M_{ac} is negative corroborating an L^- domain state. The L^- domains are stabilized by the antiferromagnetic coupling of Cr_2O_3 surface ions to Co spins.

The amplitude of M_{ac} increased by increasing the sensing voltage V_{sense}, whereas M_{dc} remained unchanged as expected from the absence of an ME effect in Co. The dependence of M_{ac} on V_{sense} showed a linear response indicating that the magnetoelectric effect is indeed linear [Fig. 4(b)].

APPENDIX B: CHARACTERISTICS OF THE SAMPLE WITH EXCHANGE-BIAS

The exchange bias H_{ex} was measured from the shift in the magnetization hysteresis loop of the Co layer using the reciprocating sample option of the SQUID magnetometer. The exchange-bias data were acquired from a sample that was prepared under the same fabrication conditions as the sample wEB. Figure 5(a) shows the temperature dependence of exchange-bias field H_{ex} and coercivity H_c. The low-temperature limit of H_{ex} was 570 Oe, corresponding to $J_K = 8\times10^{-3}\mathrm{erg/cm^2}$.

In the main text of the paper, α_{peak} was used as the main indication of the average domain state $\langle L\rangle$. The measurement of α is related to the bulk domain state. An indirect measurement is the exchange bias on the ferromagnetic layer, which is representative of the domain state at interface. Here we compare both methods.

Figures 5(b) and 5(c) show the switching of $\langle L\rangle$ after MFC in H_{fr} with a zero E_{fr}. Figure 5(b) shows the switching measured by H_{ex} at 240 K. In the intermediate switching region

2–4 kOe, the Cr_2O_3 film is composed of a large number of L^+ and L^- domains, and the exchange bias on the Co layer is weaker than the exchange stiffness of Co. Therefore, the normalized H_{ex} can be treated as the total average $\langle L\rangle$ [47]. The solution to Eq. (5) of the main text in the absence of an electric field during cooling gives:

$$\langle L\rangle = \tanh\left(\frac{H_{fr} - H_{E0}}{\lambda_H}\right), \tag{B1}$$

where

$$H_{E0} = \frac{J_K}{M_0 t}, \tag{B2}$$

and

$$\lambda_H = \frac{2k_B T_N}{M_0 V}. \tag{B3}$$

The fittings to Eq. (B1) are shown as solid lines, where the fitting values are inside the boxes. The two measurement methods of Figs. 5(b) and 5(c) are in a good agreement. The coercivity of Co H_c has a maximum at H_{E0}, where an equal number of L^+ and L^- domains are present [Fig. 5(b), with a red dashed line as an eye guide].

APPENDIX C: COUPLING OF THE ANTIFERROMAGNETIC DOMAINS AND THE SPONTANEOUS MAGNETIZATION OF SPUTTERED FILMS

In the main text, it is shown that the spontaneous magnetization M_0 and the AFM vector point in the same direction. To find how strong this spontaneous magnetization is coupled to AFM vector, we checked the effect of an external magnetic field on the switching of AFM domains in the sample woEB [Fig. 6(a)]. After MFC at a certain H_{fr}, a field in the opposite direction was applied, then α and M were measured while the temperature was increased at a heating rate of +0.5 K/min [Fig. 6(b)]. After MFC at +10 kOe, a field of −30 kOe was set and α-T dependence was measured. α changed from positive to negative values during the temperature increase [black circles in Fig. 6(c)]. Comparing with the measurements at zero field [dashed lines in Fig. 6(c)], we can say that the change corresponds to switching from L^+ to L^-. The same opposite results were found for −10-kOe MFC and subsequent +30-kOe measurement [red circles in Fig. 6(c)].

The M-T dependence could not be measured directly due to the large diamagnetic background of the substrate. We resorted to the procedure of Ref. [48], by applying the opposing magnetic field up to a certain temperature T', then cooling to 270 K and measuring TRM at a zero field [Fig. 6(b)]. The temperature overshoot at T' was minimized to <0.6 K. The switching of M against T' was at the same temperature as α [squares in Fig. 6(c)]. This confirms that l switches together with M.

The switching temperature T_{sw} corresponds to the coercive field H_c at that temperature, and the dependence shows a large temperature variation similar to Ref. [48] [Fig. 6(d)]. This large variation is likely due to the large decrease of uniaxial magnetocrystalline anisotropy near T_N [49]. As the thermal energy increases and anisotropy decreases, the thermally activated switching occurs when anisotropy K_u becomes on same order of magnitude as the Zeeman energy of Cr_2O_3 magnetization $H \cdot M_0$.

We conclude by restating that l is parallel to M_0 [Fig. 6(e)].

[1] H. Ohno, D. Chiba, F. Matsukura, T. Omiya, E. Abe, T. Dietl, Y. Ohno, and K. Ohtani, Nature (London) **408**, 944 (2000).

[2] D. Chiba, M. Yamanouchi, F. Matsukura, and H. Ohno, Science **301**, 943 (2003).

[3] P. Borisov, A. Hochstrat, X. Chen, W. Kleemann, and C. Binek, Phys. Rev. Lett. **94**, 117203 (2005).

[4] M. Weisheit, S. Fähler, A. Marty, Y. Souche, C. Poinsignon, and D. Givord, Science **315**, 349 (2007).

[5] X. He, Y. Wang, N. Wu, A. N. Caruso, E. Vescovo, K. D. Belashchenko, P. A. Dowben, and C. Binek, Nat. Mater. **9**, 579 (2010).

[6] M. Endo, S. Kanai, S. Ikeda, F. Matsukura, and H. Ohno, Appl. Phys. Lett. **96**, 212503 (2010).

[7] D. Chiba, S. Fukami, K. Shimamura, N. Ishiwata, K. Kobayashi, and T. Ono, Nat. Mater. **10**, 853 (2011).

[8] Y. Shiota, T. Nozaki, F. Bonell, S. Murakami, T. Shinjo, and Y. Suzuki, Nat. Mater. **11**, 39 (2011).

[9] F. Matsukura, Y. Tokura, and H. Ohno, Nat. Nanotechnol. **10**, 209 (2015).

[10] M. Fiebig, J. Phys. D: Appl. Phys. **38**, R123 (2005).

[11] W. Eerenstein, N. D. Mathur, and J. F. Scott, Nature (London) **442**, 759 (2006).

[12] S. M. Wu, S. A. Cybart, D. Yi, J. M. Parker, R. Ramesh, and R. C. Dynes, Phys. Rev. Lett. **110**, 067202 (2013).

[13] J. T. Heron, J. L. Bosse, Q. He, Y. Gao, M. Trassin, L. Ye, J. D. Clarkson, C. Wang, J. Liu, S. Salahuddin, D. C. Ralph, D. G. Schlom, J. Íñiguez, B. D. Huey, and R. Ramesh, Nature (London) **516**, 370 (2014).

[14] T. Ashida, M. Oida, N. Shimomura, T. Nozaki, T. Shibata, and M. Sahashi, Appl. Phys. Lett. **106**, 132407 (2015).

[15] C. Binek and B. Doudin, J. Phys.: Condens. Matter **17**, L39 (2005).

[16] M. Matsuzaki, K. Shinohara, T. Shibata, M. Sahashi, and T. Nozaki, Magnetic recording system and magnetic recording device, U.S. Patent App. 13/839,163, 2014 .

[17] T. Shibata and M. Sahashi, Magnetization controlling element using magnetoelectric effect, U.S. Patent App. 14/532,533, 2015.

[18] I. Dzyaloshinskii, Sov. Phys. JETP **10**, 628 (1960).

[19] D. N. Astrov, Sov. Phys. JETP **11**, 708 (1960).

[20] T. H. O'Dell, *The Electrodynamics of Magneto-Electric Media* (North-Holland, Amsterdam, 1970).

[21] Y. Shiratsuchi, T. Fujita, H. Noutomi, H. Oikawa, and R. Nakatani, IEEE Trans. Magn. **47**, 3909 (2011).

[22] S. P. Pati, N. Shimomura, T. Nozaki, T. Shibata, and M. Sahashi, J. Appl. Phys. **117**, 17D137 (2015).

[23] N. Shimomura, S. P. Pati, T. Nozaki, T. Shibata, and M. Sahashi, AIP Adv. **7**, 025212 (2017).

[24] S. P. Pati, M. Al-Mahdawi, S. Ye, Y. Shiokawa, T. Nozaki, and M. Sahashi, Phys. Rev. B **94**, 224417 (2016).

[25] T. Ashida, M. Oida, N. Shimomura, T. Nozaki, T. Shibata, and M. Sahashi, Appl. Phys. Lett. **104**, 152409 (2014).

[26] K. Toyoki, Y. Shiratsuchi, A. Kobane, S. Harimoto, S. Onoue, H. Nomura, and R. Nakatani, J. Appl. Phys. **117**, 17D902 (2015).

[27] K. Toyoki, Y. Shiratsuchi, A. Kobane, C. Mitsumata, Y. Kotani, T. Nakamura, and R. Nakatani, Appl. Phys. Lett. **106**, 162404 (2015).

[28] K. Toyoki, Y. Shiratsuchi, T. Nakamura, C. Mitsumata, S. Harimoto, Y. Takechi, T. Nishimura, H. Nomura, and R. Nakatani, Appl. Phys. Express **7**, 114201 (2014).

[29] P. Borisov, T. Ashida, T. Nozaki, M. Sahashi, and D. Lederman, Phys. Rev. B **93**, 174415 (2016).

[30] Y. Shiratsuchi and R. Nakatani, Mater. Trans. **57**, 781 (2016).

[31] T. Kosub, M. Kopte, F. Radu, O. G. Schmidt, and D. Makarov, Phys. Rev. Lett. **115**, 097201 (2015).

[32] T. Kosub, M. Kopte, R. Hühne, P. Appel, B. Shields, P. Maletinsky, R. Hübner, M. O. Liedke, J. Fassbender, O. G. Schmidt, and D. Makarov, Nat. Commun. **8**, 13985 (2017).

[33] K. D. Belashchenko, O. Tchernyshyov, A. A. Kovalev, and O. A. Tretiakov, Appl. Phys. Lett. **108**, 132403 (2016).

[34] K. D. Belashchenko, Phys. Rev. Lett. **105**, 147204 (2010).

[35] P. J. Brown, J. B. Forsyth, and F. Tasset, J. Phys.: Condens. Matter **10**, 663 (1998).

[36] M. Al-Mahdawi, Y. Shiokawa, S. P. Pati, S. Ye, T. Nozaki, and M. Sahashi, J. Phys. D: Appl. Phys. **50**, 155004 (2017).

[37] G. T. Rado, Phys. Rev. Lett. **6**, 609 (1961).

[38] M. Mostovoy, A. Scaramucci, N. A. Spaldin, and K. T. Delaney, Phys. Rev. Lett. **105**, 087202 (2010).

[39] P. Borisov, A. Hochstrat, V. V. Shvartsman, and W. Kleemann, Rev. Sci. Instrum. **78**, 106105 (2007).

[40] L. Fallarino, C. Binek, and A. Berger, Phys. Rev. B **91**, 214403 (2015).

[41] P. J. Brown, J. B. Forsyth, E. Lelièvre-Berna, and F. Tasset, J. Phys.: Condens. Matter **14**, 1957 (2002).

[42] Y. Shiratsuchi, Y. Kotani, S. Yoshida, Y. Yoshikawa, K. Toyoki, A. Kobane, R. Nakatani, and T. Nakamura, AIMS Mater. Sci. **2**, 484 (2015).

[43] J. A. Mejias, V. Staemmler, and H.-J. Freund, J. Phys.: Condens. Matter **11**, 7881 (1999).

[44] X.-G. Wang, A. Chaka, and M. Scheffler, Phys. Rev. Lett. **84**, 3650 (2000).

[45] J. A. Hertz and M. A. Klenin, Physica B + C **91**, 49 (1977).

[46] T. Moriya, J. Phys. Soc. Jpn. **51**, 420 (1982).

[47] T. Nozaki, M. Al-Mahdawi, S. P. Pati, S. Ye, and M. Sahashi, Appl. Phys. Lett. **110**, 132408 (2017).

[48] L. Fallarino, A. Berger, and C. Binek, Appl. Phys. Lett. **104**, 022403 (2014).

[49] S. Foner, Phys. Rev. **130**, 183 (1963).